Dynamic analysis of fretting-wear in friction contact interfaces

L. Salles [a,b,c], L. Blanc [a,*], F. Thouverez [a], A.M. Gouskov [b]

[a] *École Centrale de Lyon, Laboratoire de Tribologie et Dynamique des Systèmes, Équipe Dynamique des Structures et des Systèmes, 36 Avenue Guy de Collongue, 69134* Ecully, France

[b] *Department of Applied Mechanics, Bauman Moscow State Technical University, Moscow, Russia*

[c] *Snecma – Safran group, 77550 Moissy-Cramayel, France*

A B S T R A C T

A numerical treatment of fretting-wear under vibratory loading is proposed. The method is based on the Dynamic Lagrangian Frequency Time method. It models unilateral contact by using Coulomb's friction law. The basic idea is to separate time into two scales, a slow scale for tribological phenomena and a fast scale for dynamics. For a given number of vibration periods, a steady state is assumed and the variables are decomposed into Fourier series. An Alternating Frequency Time procedure is performed to calculate the non-linear forces. Then, a hybrid Powell solver is used. Numerical investigations on a beam with fric-tion contact interfaces illustrate the performances of this method and show the coupling between dynamic and tribological phenomena.

1. Introduction

Friction dampers are widely used in industry and civil engineering to control the vibrations of structures. Friction damping is often obtained via the design of the mechanism, which is the case, for example, in turbomachinery applications when a bladed disk includes dovetail attachments. The positive effect of such dampers is that they decrease vibrations, but friction also introduces micro and/or macro slip that can be accompanied by fretting-wear. Indeed, some aeronautical companies have observed that the predictions underestimate wear on the dovetail profiles of long-haul aircraft. However, this problem has not been encountered on short-haul aircraft equipped with the same type of engines. Considering that wear predictions have been performed in quasi-static take-off and landing situations, for which vibratory effects are neglected, it is presumed here that coupling between wear and vibrations occurs during the portions of the flights occurring at cruising speed, which is especially true since these operating modes last much longer for long-haul aircraft than other types. An academic example is proposed to illustrate the most pertinent phenomena.

Roughly speaking, the state of the art concerning the modeling and calculation methods available for solving such problems is as follows. On the one hand, recent methods enable the calculation of vibrational response of bladed disks in the presence of friction in blade attachments (Charleux et al., 2006; Petrov and Ewins, 2003; Nacivet et al., 2003), but wear is not taken into account; on the other hand, most fretting-wear studies are performed in quasi-static situations for which inertial – and thus vibratory – effects are neglected. Apart from Levy (1980), and Sextro (2002), coupling between fretting-wear and vibrations is very seldom taken into account in the literature, due to the complexity it introduces. Nevertheless, certain experimental studies have investigated the effect of frequency on fretting wear (Berthier et al., 1988; Soderberg et al., 1986; Leonard et al., 2009).

Wear itself is a complex phenomenon because wear debris can depend on hardness, plasticity, grain structure, temperature, etc. According to (Meng and Ludema, 1995), about 180 wear laws have been proposed. Archard's model (Archard, 1953) is that most commonly used to quantify wear. It considers that the wear volume is linked to the product of normal force and sliding velocity. Wear coefficient quantification is conventionally performed by evaluating the worn volume as a function of normal load. The loss of material can be known by measuring loss of mass, loss of dimensions, the evolution of Vickers microhardness imprints, or directly by surface profilometry. The Archard model will be used here.

In the absence of vibratory effects, wear laws are often used with the Finite Element Method (FEM) as post-processing steps in looping procedures to solve deformable contact problems and obtain the evolution of wear rates and worn geometries. Commercial software can be used to model wear-cycles with an external routine to compute wear and remesh the geometry (McColl et al., 2004; Mary and Fouvry, 2007). This strategy is highly time-consuming. In order to reduce calculation costs, several simplified approaches have been developed based on Winkler's foundation to predict wear (Põdra and Andersson, 1997). Various approaches have also been proposed to predict wear based on semi-analytical models (Gallego et al., 2006) or on Boundary Element Methods

Nomenclature

U	vector of nodal displacements	$-_N$	normal quantity
W	vector of nodal wear depths	$-_T$	tangential quantity
X	vector of nodal displacements (satisfying the contact laws)	$\tilde{-}$	multiharmonic vector
		$-_M$	quantity relative to node M
Z	dynamic stiffness	$-^n$	relative to instant n of a vibration period
$\boldsymbol{\lambda}$	contact force	$-_U$	evaluated thanks to the **U** given by a Newton solver iteration
ϵ	penalty coefficient		
k_w	Archard's law wear coefficient	$-_x$	correction added to a $-_U$ quantity to match the contact laws
μ	Coulomb friction coefficient		
$-_r$	quantity linked to relative displacements	$-_{pre}$	predicted quantity

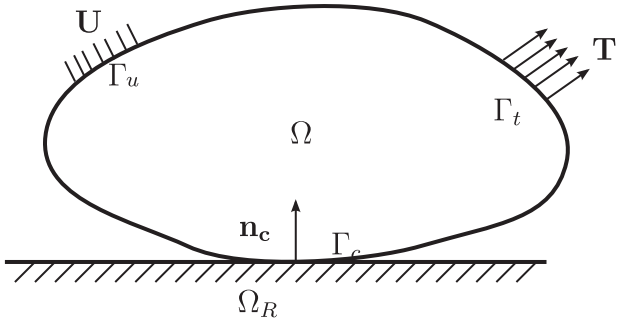

Fig. 1. Description of the problem.

(BEM) (Sfantos and Aliabadi, 2006). The latter method has been coupled with an optimization technique (Sfantos and Aliabadi, 2006) to obtain worn geometry directly.

In this paper, an approach based on the FEM is proposed to model the coupling between fretting-wear and vibration. It is based on the Dynamic Lagrangian Frequency Time method (DLFT) (Nacivet et al., 2003) and on a multiscale approach to reduce computational costs. The main assumption is that a periodic steady state is reached and that wear will modify this state only slightly. Thus it is possible to use methods based on Multi Harmonic Balance and Alternate Frequency Time procedures (Guillen et al., 1999; Csaba, 1998; Petrov and Ewins, 2003). Multiscale formalism is introduced to distinguish between the "fast" phenomena caused by vibrations and the "slow" phenomena due to wear. It is then necessary to implement iterative numerical techniques, because a non-linear system must be solved at each step of the slow scale. Here the strategy is based on a hybrid Powell solver. Concerning the treatment of wear through Archard's law, it is assumed that the friction coefficient is unaffected by the evolution of wear. Hardness will be considered constant. The plasticity of the material will be neglected. However, more elaborate models, for example, based on the dissipated energy (Fouvry et al., 2003), could also have been used.

The first examples treated by this DLFT-with-wear method were reported in Salles et al. (2008) and Salles et al. (2009). Here the formalism is presented more thoroughly and a comparison with an example from the literature is proposed (Stromberg, 1997).

2. The reference problem

2.1. Continuous formulation

Let us consider an elastic solid Ω in contact with a fixed rigid body Ω_R through a frictional interface Γ_c in a situation of fretting-wear (Fig. 1). The boundary of Ω, $\partial\Omega$, is smooth; it is divided into three disjoint parts Γ_t, Γ_u and Γ_c. $\mathbf{n}$ designates the unit normal vector outward from $\partial\Omega$. Traction forces **T** excite Γ_t periodically. Displacements **U** are imposed on Γ_u and frictional contact with fretting-wear conditions on Γ_c. There are no body forces. The constitutive law associated with Ω is elastic, linear and isotropic. Disturbances are assumed to be small.

In the case of inertial forces, the elasticity equations for Ω, excepting the contact interface, are, conventionally:

$$\mathbf{div}\boldsymbol{\sigma} = \rho\ddot{\mathbf{u}} \quad \text{in } \Omega, \tag{1}$$

$$\boldsymbol{\sigma}\mathbf{n} = \mathbf{T} \quad \text{on } \Gamma_t, \tag{2}$$

$$\mathbf{u} = \mathbf{U} \quad \text{on } \Gamma_u, \tag{3}$$

$$\boldsymbol{\sigma} = \mathbf{E}\boldsymbol{\epsilon} \quad \text{in } \Omega, \tag{4}$$

where **u**, $\boldsymbol{\sigma}$, **E** and $\boldsymbol{\epsilon}$ are respectively the field of displacements, Cauchy's stress tensor, Hooke's tensor and the linearized Euler–Lagrange strain tensor.

According to Stromberg's conclusions (Stromberg, 1997), the constitutive equations ruling the contact interface are as follows.

- Firstly, an extension of Signorini's unilateral contact conditions takes wear into account. u_N designates the normal component of the interfacial displacement. Wear is introduced as variable w, increasing the initial gap g between the two surfaces in contact. The unilateral contact conditions are:

$$\mathcal{W} = p_N \geqslant 0, \quad u_N - w - g \leqslant 0, \quad p_N(u_N - w - g) = 0, \tag{5}$$

where $\mathcal{W}$ designates the dual of w, i.e. the driving force for wear, which has the same physical meaning as p_N, the normal component of the contact pressure applied by Ω_R on Ω.
- Secondly Coulomb's law takes friction into account and Archard's law gives an estimate of wear. $\mathbf{p_T}$ is the tangential component of the contact pressures. $\|\cdot\|$ represents the Euclidian norm. μ and k_w are respectively Coulomb's friction coefficient and Archard's law wear coefficient. The complementary laws for $\mathcal{W} = p_N \geqslant 0$ are:

$$\begin{aligned} &\dot{\mathbf{u}}_T = \dot{\lambda}\frac{\mathbf{p_T}}{\|\mathbf{p_T}\|}, \quad \dot{w} = \dot{\lambda}k_w p_N, \\ &\dot{\lambda} \geqslant 0, \quad \|\mathbf{p_T}\| - \mu p_N \leqslant 0, \quad \dot{\lambda}(\|\mathbf{p_T}\| - \mu p_N) = 0 \end{aligned} \tag{6}$$

Eq. (6) shows both a local form of Archard's law of wear and a mathematical definition of Coulomb's cone in the case of fretting-wear.

Variationally, the problem is defined by three integral equations and one constitutive law (Eqs. (7)–(10)). These equations stem from the principle of virtual work, the weak formulation of Signorini's unilateral contact conditions, Coulomb's complementary law and the local formulation of Archard's law. For each moment t of the time interval $[0,T]$ studied, the displacement field **u** for each

point $\mathbf{x}$ of Ω and the contact pressure field $\mathbf{p}$ (with $p_N = \mathcal{W}$ and $\mathbf{p_T}$ its normal and tangential components) are sought. $\mathbf{v}$, $\mathbf{p}'$ and $\mathcal{W}'$ designate the test-fields associated with $\mathbf{u}$, $\mathbf{p}$ and $\mathcal{W}$, respectively.

$$\int_{\Omega^l} \rho \ddot{u}_i v_i dV + \int_{\Omega^l} E_{ijkl} \frac{\partial u_k}{\partial x_l} \frac{\partial v_i}{\partial x_j} dV + \int_{\Gamma_c} p_i v_i dA - \int_{\Gamma_t^l} t_i v_i dA = 0 \quad \forall \mathbf{v} \in \mathcal{V}, \tag{7}$$

$$\int_{\Gamma_c} (u_N - w - g)(p'_N - p_N) dA \leqslant 0 \quad \forall p'_N \in \mathcal{K}_N, \tag{8}$$

$$\int_{\Gamma_c} (\dot{u}_{T_\alpha}(p'_{T_\alpha} - p_{T_\alpha}) + \dot{w}(\mathcal{W}' - \mathcal{W})) dA \leqslant 0 \quad \forall (p'_T, \mathcal{W}') \in \mathcal{F}(p_N) \tag{9}$$

with

$$\mathcal{V} = \{\mathbf{v} | \mathbf{v}(\mathbf{x}) = \mathbf{0}, \mathbf{x} \in \Gamma_u\},$$

$$\mathcal{K}_N = \{p_N | p_N(\mathbf{x}) \geqslant 0, \mathbf{x} \in \Gamma_c\},$$

$$\mathcal{F}(p_N) = \{(\mathbf{p_T}, \mathcal{W}) : \|\mathbf{p_T}\| - \mu p_N + {}_w p_N \mathcal{W} - k_w p_N^2 \leqslant 0, \mathbf{x} \in \Gamma_c\}.$$

In Eq. (9), the components of each vector are expressed in an orthonormal basis $\mathbf{n}_\alpha$, perpendicular to $\mathbf{n}$. $\dot{w}$ is obtained through the following equation:

$$\dot{w} = k_w |p_N| \|\dot{\mathbf{u}}_T\| \tag{10}$$

2.2. Finite element discretization

An FEM discretization of Eq. (7) is performed. Capital letters designate the FEM counterpart of the variables previously named by small letters: they are vectors of nodal quantities. The equations of motion are:

$$\mathbf{M}\ddot{\mathbf{U}} + \mathbf{C}\dot{\mathbf{U}} + \mathbf{K}\mathbf{U} + \mathbf{F_c}(\mathbf{U}, \dot{\mathbf{U}}, \mathbf{W}) = \mathbf{F_{ex}}, \tag{11}$$

where $\mathbf{M}$, $\mathbf{C}$ and $\mathbf{K}$ respectively designate the mass, damping and stiffness matrices. $\mathbf{F_{ex}}$ is the vector of external forces. $\mathbf{F_c}$ represents the non-linear contact forces due to friction and impact; they also depend on wear and on the properties of the materials.

Wear is calculated at each interface node by:

$$\dot{W}^M = k_w \left| P_N^M \right| \left\| \dot{\mathbf{U}}_T^M \right\|. \tag{12}$$

Exponent M in P_N^M and $\dot{\mathbf{U}}_T^M$ designate the nodal quantities.

The constraints introduced by Eqs. (8) and (9) become:

$${}^{\mathbf{t}}(\mathbf{U}_N - \mathbf{W} - \mathbf{G})(\mathbf{P}'_N - \mathbf{P}_N) \leqslant 0 \quad \forall \mathbf{P}'_N \in \mathcal{K}_N^h, \tag{13}$$

$${}^{\mathbf{t}}\dot{\mathbf{U}}_T(\mathbf{P}'_T - \mathbf{P}_T) \leqslant 0 \quad \forall \mathbf{P}'_T \in \mathcal{F}^h(\mathbf{P}_N), \tag{14}$$

where $\mathcal{K}_N^h = \left\{P_N^M | P_N^M \geqslant 0\right\}$ is the approximation of $\mathcal{K}_N$ and $\mathcal{F}^h(\mathbf{P}_N) = \left\{\mathbf{P}_T^M | \left\|\mathbf{P}_T^M\right\| - \mu \left|\mathbf{P}_N^M\right| \leqslant 0\right\}$ is the approximation of $\mathcal{F}(p_N)$ with $\mathcal{W}^M = \mathbf{P}_N^M$.

3. The "DLFT with wear" method

3.1. A harmonic balance method with two time scales

The strategy belongs to the family of multiscale approaches (Nayfeh and Mook, 1979; Meirovitch, 2004). In Cusumano and Chatterjee (2000), a time scale separation is also used with an averaging procedure to qualitatively estimate the dynamics of the change in damage. The wear of a wheel-rail is studied this way in Demiray and Brommundt (1997).

Here, time is split into two different scales: a fast scale associated with vibratory phenomena and a slow one associated with wear. τ and η are the variables of the fast and slow time scales respectively. At the scale of a few cycles, wear appears to be an almost constant interface gap. It is therefore assumed that wear does not change the appearance of the periodic response during a short lapse of time: in this period it is possible to describe displacements and forces with Fourier series of τ. For a longer duration, Fourier coefficients evolve as functions of η. Whatever the case, wear does not change the pulsation of the response because it is governed by the pulsation of the excitation, ω, which is not affected by fretting-wear. η is associated with a much longer time scale than the time period $T_f = \frac{2\pi}{\omega}$ of the fretting-wear cycles.

The Fourier series of $\mathbf{U}$ can be expressed as:

$$\mathbf{U}(\tau, \eta) = \widetilde{\mathbf{U}}_0(\eta) + \sum_{n=1}^{N_h} \left(\widetilde{\mathbf{U}}_{n,c}(\eta) \cos(n\omega\tau) + \widetilde{\mathbf{U}}_{n,s}(\eta) \sin(n\omega\tau)\right). \tag{15}$$

Then, Eq. (15) is summarized by a multi-harmonic frequency-domain vector:

$$\widetilde{\mathbf{U}}(\eta) = \left[\widetilde{\mathbf{U}}_0, \widetilde{\mathbf{U}}_{1,c}, \cdots, \widetilde{\mathbf{U}}_{N_h,c}, \widetilde{\mathbf{U}}_{1,s}, \cdots, \widetilde{\mathbf{U}}_{N_h,s}\right], \tag{16}$$

where c and s respectively stand for "cosine" and "sine".

A Galerkin procedure is then performed to formulate Eq. (11) in the frequency domain. It is important to mention that, here, the depth of wear is very small compared with the characteristic dimensions of the structures in contact; this is why the modifications of the mass and stiffness matrices due to wear are neglected. Eq. (11) becomes:

$$\mathbf{Z}\widetilde{\mathbf{U}}(\eta) + \widetilde{\mathbf{F}}_c(\eta) = \widetilde{\mathbf{F}}_{ex}(\eta). \tag{17}$$

$\widetilde{\mathbf{F}}_c$ and $\widetilde{\mathbf{F}}_{ex}$ are respectively the multi-harmonic frequency-domain vectors of contact and excitation forces. $\mathbf{Z}$ is a block-diagonal matrix such that:

$$\mathbf{Z} = diag(\mathbf{K}, \mathbf{Z}_1, \ldots, \mathbf{Z}_{N_h}) \text{ with}$$

$$\mathbf{Z}_n = \begin{bmatrix} \mathbf{K} - (n\omega)^2\mathbf{M} & n\omega\mathbf{C} \\ -n\omega\mathbf{C} & \mathbf{K} - (n\omega)^2\mathbf{M} \end{bmatrix}, \quad n = 1 \ldots N_h \tag{18}$$

In practice, as described in Nacivet et al. (2003), the size of the frequency-domain problem is reduced, without loss of information, by condensation on the interface nodes. These are involved later in the treatment of contact non-linearities. Eq. (17) becomes:

$$\mathbf{Z_r}\widetilde{\mathbf{U}}_r(\eta) + \tilde{\lambda}(\eta) = \widetilde{\mathbf{F}}_r, \tag{19}$$

or

$$f(\widetilde{\mathbf{U}}_r) = \mathbf{Z_r}\widetilde{\mathbf{U}}_r(\eta) + \tilde{\lambda}(\eta) - \widetilde{\mathbf{F}}_r = \mathbf{0}, \tag{20}$$

where $\widetilde{\mathbf{U}}_r$, $\widetilde{\mathbf{F}}_r$ and $\mathbf{Z}_r$ designate the reduced multiharmonic relative displacement vector, reduced stiffness matrix and reduced external excitation respectively. $\tilde{\lambda}$ is the vector of the reduced contact forces in the frequency domain.

Algorithmically, the solution over the time interval $[0, T]$ is calculated through a step-by-step procedure involving an incrementation of the slow time variable: for each step, Eq. (20) is solved by a Newton solver; this process constitutes the external loop of the method (see Fig. 2).

3.2. Modeling of the contact forces

Solving Eq. (19) requires knowing the expression of $\tilde{\lambda}$. Unfortunately, it is not possible to calculate it directly in the Galerkin

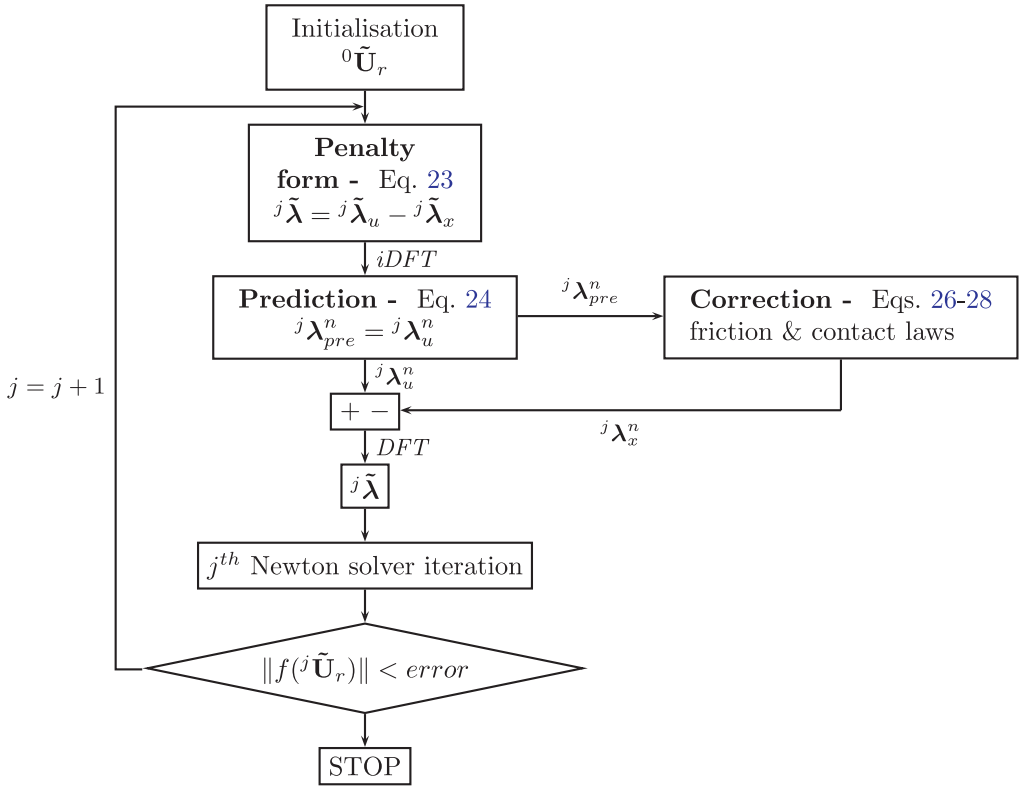

Fig. 2. Implementation of the DLFT.

procedure, indeed it depends on the state of each contact node – stick, slip or separation – which is, a priori, unknown. To overcome this difficulty it is common to use the Alternating Frequency Time method (AFT) (Cameron and Griffin, 1989). Displacements and velocities are calculated in the frequency domain and transformed into the time domain by using an inverse DFT procedure (iDFT). In the time domain, contact forces can be evaluated through different methods. The easiest of these is to regularize the *sign* function, depending on the velocity in the evaluation of Coulomb's forces, by another function that is continuous. This allows the direct computation of the non-linear friction forces (Petrov and Ewins, 2002). The use of a penalty method is another popular method (Guillen et al., 1999; Petrov and Ewins, 2002; Poudou and Pierre, 2003; Petrov and Ewins, 2003; Ciğeroğlu and Özgüven, 2006; Laxalde et al., 2007). The additional stiffnesses may then represent the stiffness of a damper or that of contact asperities. In the case of fretting-wear these stiffnesses may change with the wear process, to take into account the modification of material properties in the contact area.

Another method has been proposed by Nacivet et al. (2003), namely the Dynamic Lagrangian Frequency-Time method (DLFT). It uses augmented Lagrangians that allow calculating the non-smooth frictional contact law without any "softening". A time-marching procedure in the time domain is also required. Compared to the conventional contact penalty method, the main advantage of the DLFT method is that the results do not depend on any penalty coefficient when reaching convergence. This method has been successfully used to predict friction damping in blade attachments (Charleux et al., 2006) and to quantify the efficiency of friction ring dampers (Laxalde et al., 2007).

In the frequency domain, the contact force $\tilde{\lambda}$ is formulated as a penalization of the equations of motion on the tangential and normal directions (designated respectively by the *T* and *N* subscripts on quantities):

$$\tilde{\lambda}_T = \widetilde{\mathbf{F}}_{rT} - \left(\mathbf{Z_r}\widetilde{\mathbf{U}}_\mathbf{r}\right)_T + \epsilon_T\left(\widetilde{\mathbf{U}}_{rT} - \widetilde{\mathbf{X}}_{rT}\right), \tag{21a}$$

$$\tilde{\lambda}_N = \widetilde{\mathbf{F}}_{rN} - \left(\mathbf{Z_r}\widetilde{\mathbf{U}}_r\right)_N + \epsilon_N\left(\widetilde{\mathbf{U}}_{\mathbf{r}N} - \widetilde{\mathbf{W}}_N - \widetilde{\mathbf{X}}_{rN}\right). \tag{21b}$$

ϵ_T and ϵ_N are penalty coefficients, $\widetilde{\mathbf{X}}_r$ is a new vector of reduced multiharmonic relative displacements, it is introduced to designate the value taken by $\widetilde{\mathbf{U}}_\mathbf{r}$ after it has been corrected to fit the contact conditions. Indeed, the pair $\left(\tilde{\lambda}, \widetilde{\mathbf{X}}_\mathbf{r}\right)$ is determinated through an AFT procedure described below. Therefore, contrary to $\widetilde{\mathbf{U}}_\mathbf{r}$ which is evaluated through the frequencial HBM formulation of the problem at each step of the Newton solver, $\widetilde{X}_\mathbf{r}$ is computed in the time domain since the contact conditions have explicit expressions only at each given instant. Eq. (20) becomes:

$$f(\widetilde{\mathbf{U}}_\mathbf{r}) = \epsilon\left(\widetilde{\mathbf{U}}_\mathbf{r} - \widetilde{\mathbf{W}} - \widetilde{\mathbf{X}}_\mathbf{r}\right), \quad \text{with} \quad \epsilon = \epsilon_T = \epsilon_N. \tag{22}$$

Practically, it has been noted that a good choice for ϵ is to take it as being equal to the spectral radius of $\mathbf{Z}_r$. The convergence ensures that the time domain $\widetilde{X}_\mathbf{r}$ and frequency domain $\widetilde{\mathbf{U}}_\mathbf{r}$ match with respect to contact conditions.

The AFT is based on a prediction/correction procedure in the time domain (summarized in Fig. 2). Algorithmically, this is the internal loop of the method.

The contact forces are calculated in the time domain, where the transition criteria between the three possible states are easily formulated. Eq. (21) is reformulated as:

$$\tilde{\lambda} = \underbrace{\widetilde{\mathbf{F}}_\mathbf{r} - \mathbf{Z}_r\widetilde{\mathbf{U}}_\mathbf{r} + \epsilon\left(\widetilde{\mathbf{U}}_\mathbf{r} - \widetilde{\mathbf{W}}\right)}_{\tilde{\lambda}_\mathbf{u}} - \underbrace{\epsilon\widetilde{\mathbf{X}}_\mathbf{r}}_{\tilde{\lambda}_\mathbf{x}}, \tag{23}$$

where $\tilde{\lambda}_\mathbf{x}$ designates the correction sought and which must be applied to the contact forces to match the contact conditions. The period is split into *N* time steps, *n* superscripts designate instant *n*. $\tilde{\lambda}$, $\tilde{\lambda}_\mathbf{u}$ and $\tilde{\lambda}_\mathbf{x}$ have $\{\boldsymbol{\lambda}^\mathbf{n}\}_{n=1..N}$, $\{\boldsymbol{\lambda}^\mathbf{n}_\mathbf{u}\}_{n=1..N}$ and $\{\boldsymbol{\lambda}^\mathbf{n}_\mathbf{x}\}_{n=1..N}$ as respective

time domain counterparts. These vectors are obtained from the frequency domain vectors through an iDFT procedure. A prediction/correction procedure is then used to compute the contact forces. At each time increment it is first assumed that the contact node, identified by superscript M, has not moved tangentially since the former time step (entailing $\boldsymbol{\lambda}_{\mathbf{xT}}^{\mathbf{Mn}} = \boldsymbol{\lambda}_{\mathbf{xT}}^{\mathbf{M(n-1)}}$) and that the normal force has not changed ($\boldsymbol{\lambda}_{\mathbf{xN}}^{\mathbf{Mn}} = 0$). The predicted contact forces are:

$$\boldsymbol{\lambda}_{\mathbf{preT}}^{\mathbf{Mn}} = \boldsymbol{\lambda}_{\mathbf{uT}}^{\mathbf{Mn}} - \boldsymbol{\lambda}_{\mathbf{xT}}^{\mathbf{M(n-1)}}, \quad \lambda_{preN}^{Mn} = \lambda_{uN}^{Mn}. \tag{24}$$

The corrected contact forces will be:

$$\boldsymbol{\lambda}^{Mn} = \boldsymbol{\lambda}_{\mathbf{u}}^{\mathbf{Mn}} - \boldsymbol{\lambda}_{\mathbf{x}}^{\mathbf{Mn}}. \tag{25}$$

Correction $\boldsymbol{\lambda}_{\mathbf{x}}^{\mathbf{Mn}}$ is deduced from the predictions so that $\boldsymbol{\lambda}^{\mathbf{Mn}}$ satisfies the contact and friction laws, according to the three possible following situations.

1. Separation: $\lambda_{preN}^{Mn} \geqslant 0$

The contact is lost and the forces should be zero.

$$\boldsymbol{\lambda}_{\mathbf{x}}^{\mathbf{Mn}} = \boldsymbol{\lambda}_{\mathbf{u}}^{\mathbf{Mn}}. \tag{26}$$

2. Stick: $\lambda_{preN}^{Mn} < 0$ and $\left\| \boldsymbol{\lambda}_{\mathbf{preT}}^{\mathbf{Mn}} \right\| < \mu \left| \lambda_{preN}^{Mn} \right|$

In this case, the prediction verifies the contact conditions:

$$\lambda_{xN}^{Mn} = 0, \quad \boldsymbol{\lambda}_{\mathbf{xT}}^{\mathbf{Mn}} = \boldsymbol{\lambda}_{\mathbf{xT}}^{\mathbf{M(n-1)}}. \tag{27}$$

3. Slip: $\lambda_{preN}^{Mn} < 0$ and $\left\| \boldsymbol{\lambda}_{\mathbf{preT}}^{\mathbf{Mn}} \right\| \geqslant \mu \left| \lambda_{preN}^{Mn} \right|$

Again, there is no normal relative displacement. The correction is performed by assuming that the tangential contact force has the same direction as the predicted tangential force. The definition of relative velocity and Coulomb's law gives:

$$\lambda_{xN}^{Mn} = 0, \quad \boldsymbol{\lambda}_{\mathbf{xT}}^{\mathbf{Mn}} = \boldsymbol{\lambda}_{\mathbf{xT}}^{\mathbf{M(n-1)}} + \boldsymbol{\lambda}_{\mathbf{preT}}^{\mathbf{Mn}} \left(1 - \mu \frac{\left| \lambda_{preN}^{Mn} \right|}{\left\| \boldsymbol{\lambda}_{\mathbf{preT}}^{\mathbf{Mn}} \right\|} \right). \tag{28}$$

Knowing $\boldsymbol{\lambda}_{\mathbf{x}}^{\mathbf{Mn}}$ for each instant n, the final step consists of transforming the updated contact forces of the time domain back into the frequency domain by using the DFT algorithm. This gives $\tilde{\lambda}_{\mathbf{x}}$, $\widetilde{\mathbf{X}}_{\mathbf{r}}$ and thus an updated estimate of $\tilde{\lambda}$. It serves as an input for a new step in the resolution of Eq. (20) by the Newton solver. The required Jacobian matrix is evaluated quasi-analytically to reduce the computational time, following the method described in Salles et al. (2009). The process is assumed to be converged when $\|f(\widetilde{\mathbf{U}}_{\mathbf{r}})\| \leqslant \epsilon_r \|\mathbf{Z}_{\mathbf{r}} \widetilde{\mathbf{U}}_{\mathbf{r}}\|$. The relative error ϵ_r is chosen heuristically and is sufficiently small.

3.3. Wear depth calculation

After updating $\widetilde{\mathbf{U}}_{\mathbf{r}}$ by the Newton solver, nodal wear is calculated for a single fretting cycle and is denoted δW_1^M, by integrating the wear rate:

$$\delta W_1^M(\eta) = k_w \int_{\eta}^{\eta + T_f} \left| P_N^M(\tau, \eta) \right| \left\| \dot{\mathbf{U}}_T^M(\tau, \eta) \right\| d\tau. \tag{29}$$

The interface gap – i.e. the geometry – can then be updated. In practice, to accelerate the calculation by decreasing the number of slow time steps, it is necessary to jump a certain number of cycles between two steps. The duration considered in this study, T_f, is split into k intermediate slow time steps. k is chosen heuristically to provide good accuracy within a reasonable calculation time.

Concerning the evolution of wear depths, the integration follows an explicit scheme:

$$\mathbf{W}^M(\eta^{k+1}) = \mathbf{W}^M(\eta^k) + \frac{\eta^{k+1} - \eta^k}{T} \delta W_1^M(\eta^k). \tag{30}$$

The equilibrium conditions of the contact are therefore modified, which requires returning to the beginning of the prediction/correction process to re-balance them. Thus a new loop, namely the wear updating loop or intermediate loop, appears in the algorithm. This is specific to the "DLFT with wear" method (Fig. 3).

4. Numerical examples

4.1. Example used for a comparison with the literature

4.1.1. Description of the model

The algorithm developed for the coupled calculation of both the wear kinetics and the vibratory response has been applied to a beam. The same example as that studied by Stromberg (1997) is chosen, making it possible to verify the results qualitatively. The numerical values are the same and the loading is assumed to be quasi-static, i.e. the frequency is low compared to the first resonance frequency of the system and inertial phenomena are neglected. This beam is parallelepipedic with length $L = 50$ mm, width $l = 5$ mm and thickness $h = 5$ mm (Fig. 4). It is made of steel. The properties of the material are $E = 210$ GPa, $\nu = 0.3$. The structure is connected to the ground by a spring of infinite stiffness in the $\mathbf{x}$ direction. It lies on a rigid support with unilateral contact conditions. The initial gap is zero. The friction coefficient is $\mu = 0.2$ and Archard's wear coefficient is $k_w = 1.10^{-11}$ Pa-1. It is subjected to a normal load P fixed at 50 MNm-1 and to an alternating line load Q. The amplitude of Q is 20 MNm-1.

The beam is discretized into linear 2D finite elements under the assumption of plane strains. Each element has four nodes with two degrees of freedom per node. For details about Strömberg's algorithms, please see (Stromberg, 1997). Concerning the harmonic balance, it uses 7 harmonics and each cycle is discretized into 64 time-steps in the DFT correction procedures.

4.1.2. Results

The worn profiles obtained in quasi-static conditions by both methods are shown in Fig. 5. The curves match well, qualitatively. The differences at the end of the beam can be explained by the fact that a linear load evolution has been approximated by sinusoidal functions in the harmonic balance procedure.

4.2. Example used to illustrate the influence of dynamics on wear

4.2.1. Description of the model

The beam is analoguous to that used in the previous calculations but the numerical values have been changed to better illustrate the interactions between wear and vibrations. Thus $L = 100$ mm, $l = 10$ mm and $h = 10$ mm. The properties of the material remain those of steel, to which are added density $\rho = 7800$ kg m-3 and damping factor $\eta = 0.001$. However, the spring is now such that $\beta = 0.01$ MN m-1. The friction coefficient is now $\mu = 0.3$, but Archard's wear coefficient is still $k_w = 1.10^{-11}$ Pa-1. The beam is subjected to a normal load P fixed at 0.01 MPa and to a sinusoidal load Q. The amplitude of Q is 0.01 MPa. In this dynamical context, it is noteworthy that the stationary body is modeled as an undeformable solid. This not only means that its wear coefficient is much lower than that of the reciprocating body, but that its rigidity remains much higher in the frequency range considered.

Two cases are treated according to the frequency of excitation. In the first case, the loading is assumed to be quasi-static. This case is considered for the sake of comparison with the second case, for which the frequency is higher, entailing that dynamical aspects must be taken into account. For both cases, the beam is discretized in the same way as in the first example. Here, the harmonic

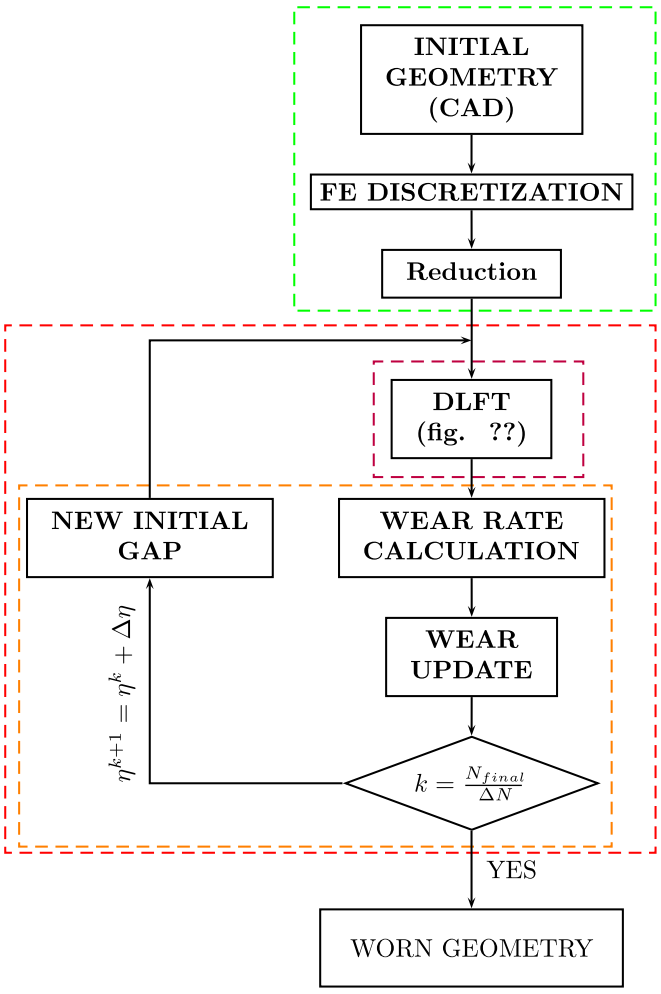

Fig. 3. Global flow chart of the "DLFT with wear" method: — model creation, — "DLFT with wear" procedure, — DLFT algorithm and — wear calculation.

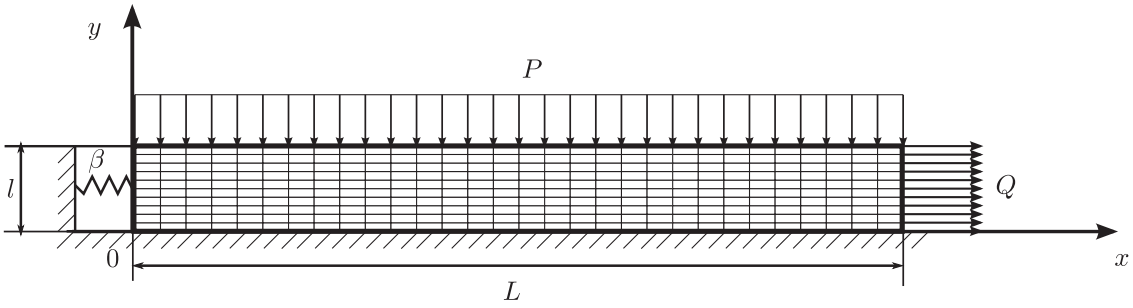

Fig. 4. Geometry, boundary conditions and mesh of the studied beam.

balance uses 7 harmonics and each cycle is discretized into 128 time-steps in the DFT correction procedures.

4.2.2. Case of a quasi-static loading

The evolution of wear depth is drawn in Figs. 6 and 7. The worn profile is drawn for the initial cycle, three intermediate numbers of cycles and for a number of cycles for which steady state has been apparently reached. Three kinds of behavior appear: no wear occurs in the zone closest to the fastening spring; maximal wear depths are reached in the zone where the oscillating load is applied; an intermediate zone separates the no-wear zone and the maximal-wear zone, and it progressively changes from stick state to slip state.

In order to better understand the wear process, the evolution of wear depth is drawn for several specific points in the slip zone (Fig. 8) and in the stick–slip zone (Fig. 9). Fig. 8 shows that in the initial slip zone wear is intense at the beginning of the process, but wear rates tend to zero when the local normal pressures relax (Figs. 10 and 11). Fig. 9 shows more complex wear kinetics. Due to the increase of wear in the sliding zone, the magnitude of the local normal pressure progressively increases in the transition zone between sticking and slipping (Figs. 10 and 11). Equilibrium conditions then cause the relaxation of the normal pressure in the sticking zone closest to the peak of normal pressure. This zone then probably becomes a sliding zone in which wear occurs. Such normal pressure redistribution phenomena mean that wear

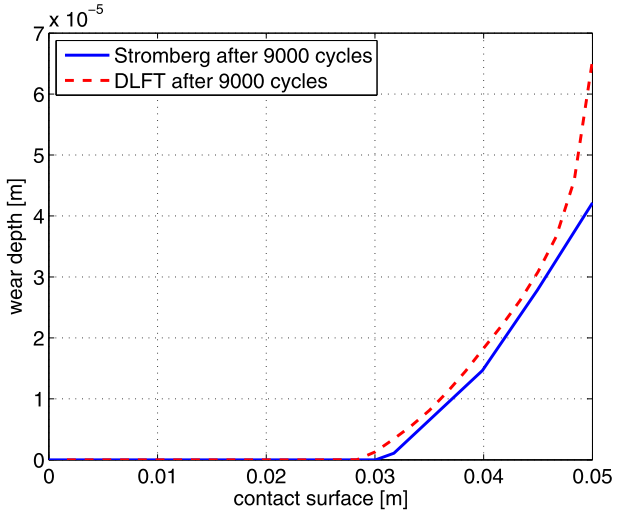

Fig. 5. Comparison of the worn profiles obtained by Strömberg's method and by the DLFT (quasi-static case).

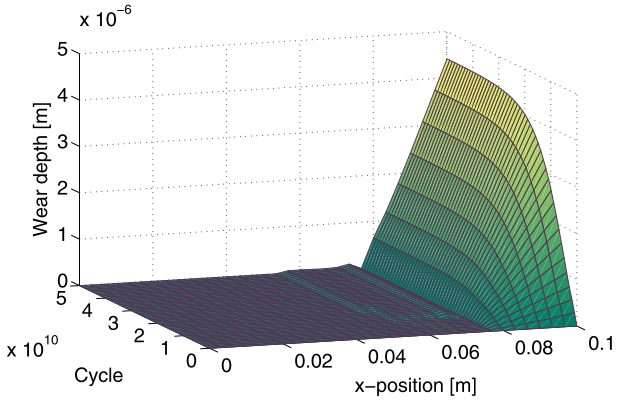

Fig. 6. Wear depth evolution (quasi-static case).

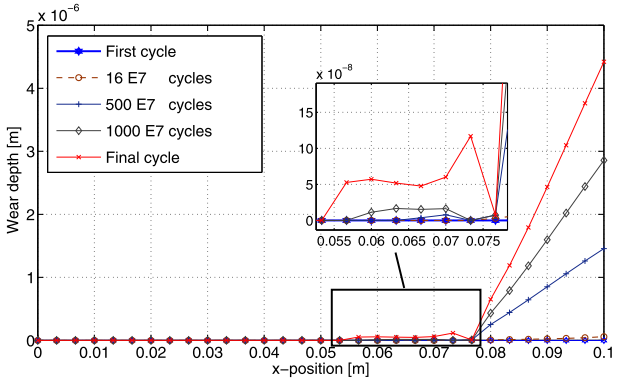

Fig. 7. Excerpt of Fig. 6: wear profile for 5 specific numbers of cycles.

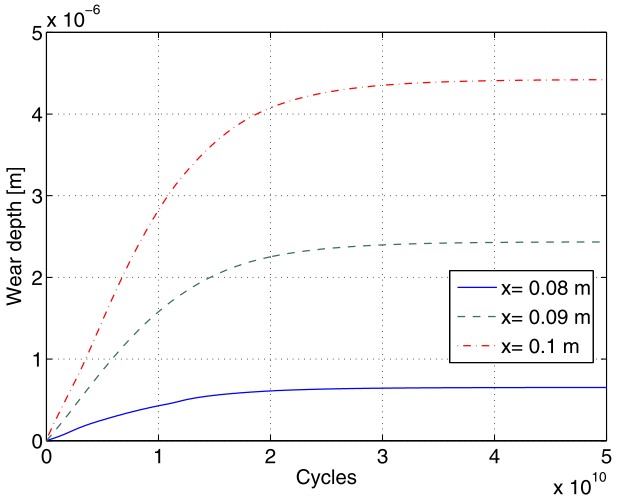

Fig. 8. Excerpt of Fig. 6: evolution of wear in the slip zone.

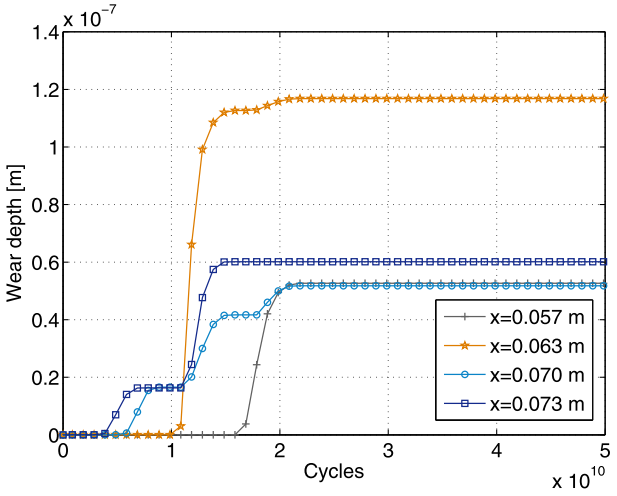

Fig. 9. Excerpt of Fig. 6: evolution of wear in the intermediate zone.

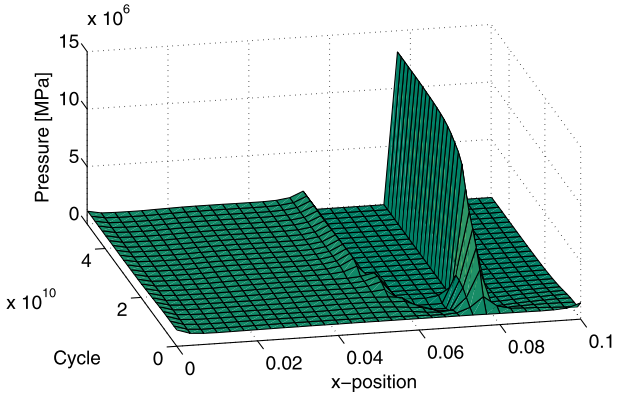

Fig. 10. Evolution of magnitude of the normal contact pressure distribution.

sometimes stops and restarts after a few cycles within a larger number of cycles.

Moreover, a small zone never seems to be subject to wear. It is characterized by null sliding (Figs. 12 and 13) and a high level of normal pressure (Fig. 11). This null-wear node plays the role of a "pillar" which could be responsible for the steady-state regime, with a null wear rate that the system seems to reach.

This example will be used in the next section as a reference while examining how inertial effects affect the wear process.

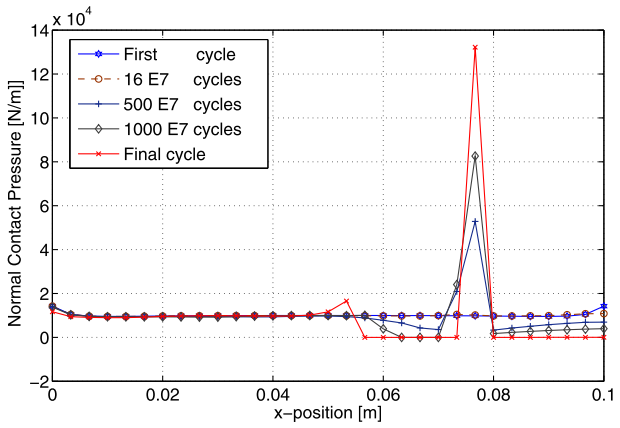

Fig. 11. Magnitude of the normal contact pressure distribution for 5 cycles (quasi-static case).

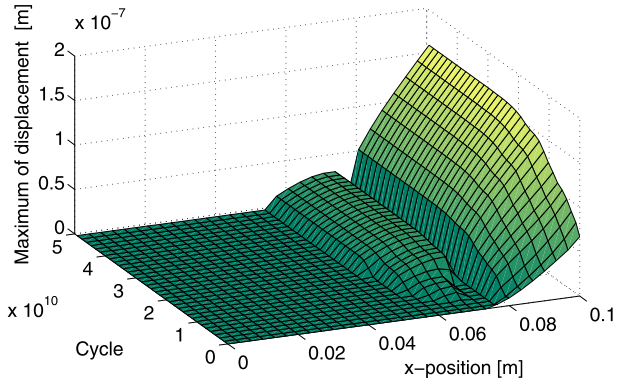

Fig. 12. Evolution of the amplitude of the horizontal displacement in the contact zone (quasi-static case, $y = 0$).

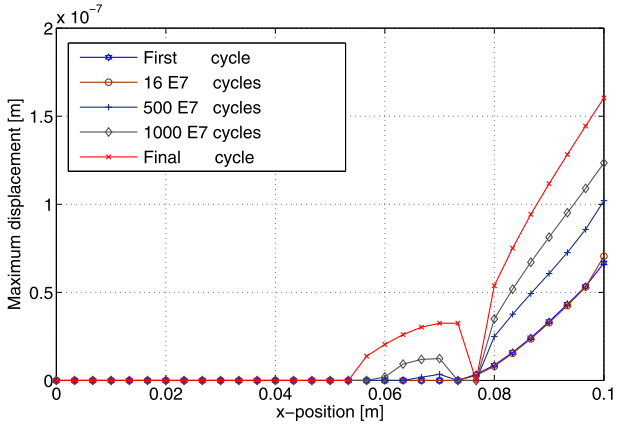

Fig. 13. Excerpt of Fig. 12: displacement amplitude for 5 particular numbers of cycles ($y = 0$).

4.2.3. Case of dynamic loadings

Initially, the vibratory behavior of the beam without wear is explored for different contact types, via the calculation of the frequency response function (FRF), giving the amplitude of the horizontal displacement at node P_e located at $(x, y) = (L, \frac{l}{2})$. The frequency range goes from 1 Hz to 100 kHz. The FRF is obtained by the DLFT algorithm (Fig. 14).

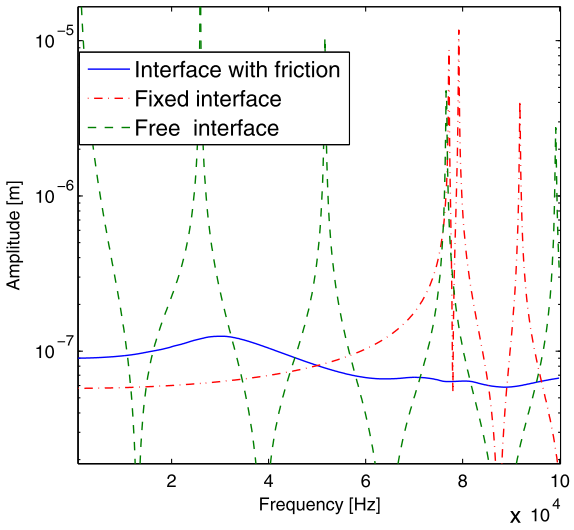

Fig. 14. FRF of the horizontal displacement of P_e with different contact types.

An additional calculation was performed to validate the choice of meshing parameters under dynamic conditions. Using only 30 contact elements in the x-direction would normally lead to an over-coarse mesh. The case with a frictional interface was therefore recalculated with 100 contact elements (Fig. 15), revealing that there was no fear of a convergence problem at FRF level.

Five modes are considered for a free interface without friction versus three modes for a fixed interface. The case with a frictional interface reveals strongly damped intermediate behavior, with resonances at 30 kHz, 70 kHz and 81 kHz (Fig. 15). Compared to the quasi-static case, the introduction of inertial effects causes different behaviors. Indeed, under sinusoidal loadings each frequency gives a different response. This is illustrated here for $f = 10$ kHz and $f = 79$ kHz (Fig. 16). The node considered previously, P_e, stops twice per period at $f = 10$ kHz and four times per period at $f = 79$ kHz. Such situations are well-known for a single degree of freedom Coulomb friction oscillator (Hong and Liu, 2000).

Wear is taken into account from this point onwards. Since the initial dynamic behavior depends on frequency, the same is true for wear: the study focuses first on excitation at $f = 79$ kHz. Computation is performed by using a simple explicit Euler scheme on the slow scale and the DLFT method for the vibratory periods.

The displacements along the contacting zone of the beam evolve according to the cycles as shown in Figs. 17 and 18: almost all the points start to move, progressively.

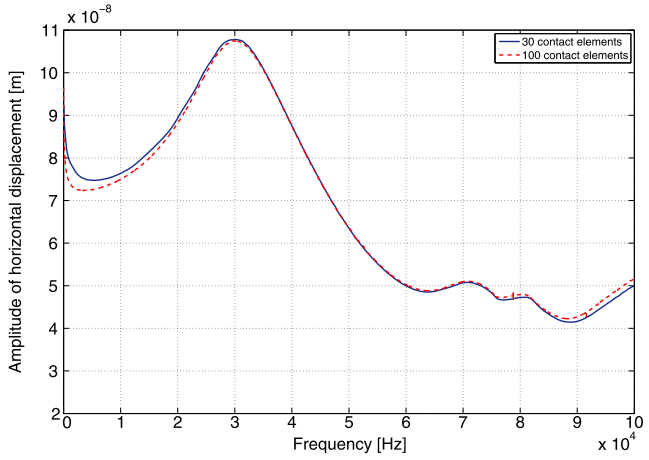

Fig. 15. FRF of the horizontal displacement with friction for two different meshes.

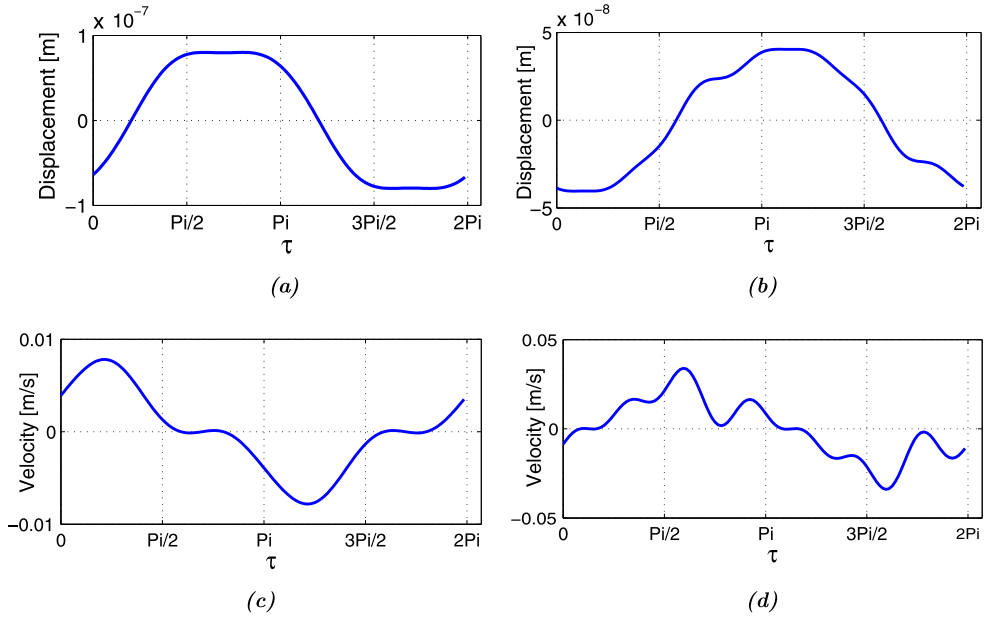

Fig. 16. Displacement and velocity of P_e versus $\tau = \omega t$: $f = 10$ kHz ((a) and (c)) and $f = 79$ kHz ((b) and (d)).

However, vibration nodes seem to appear in two zones, around $x = 0.005$ m and between $x = 0.025$ m and $x = 0.040$ m, accompanied by an increase in the magnitude of the normal contact pressure (Fig. 19) and by null wear depth (Figs. 20 and 21). The explanation of this phenomenon is analogous with that suggested in the quasi-static analysis, but here the equilibrium conditions that determine the modifications of the pressure distribution are dynamic conditions, hence the "pillar" evoked under quasi-static conditions is replaced by nodal zones of vibration. The worn geometry profile is consequently very different from that observed under quasi-static conditions.

For certain particular frequencies noted in Fig. 22, let us now calculate the worn profiles (Fig. 23).

From a physical point of view, it is noteworthy that, for the frequencies selected (those for which a peak appeared initially in the response at the end of the beam), the number of "pillars" seems to be related to the number of nodal zones in the response of the structure before wear starts. Nevertheless, it has been shown in Laxalde et al. (2008), that wear significantly affects the frequential positioning of modes and therefore the shape of the response at a fixed frequency. In our case, this phenomenon is highlighted in Fig. 24 where the FRF with frictional contact before wear occurs (already drawn on Fig. 14) is compared with that obtained after reaching a wear plateau at 79 kHz. It therefore seems risky to conclude on a general way of guessing the number and locations of "pillars" from the initial position of the nodes.

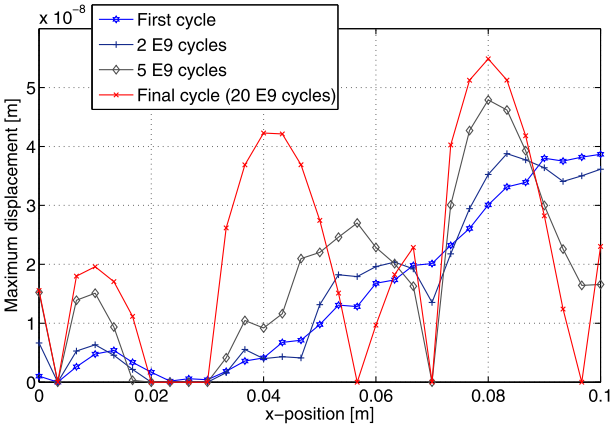

Fig. 18. Excerpt of Fig. 17: displacement amplitude for 4 cycles ($y = 0$).

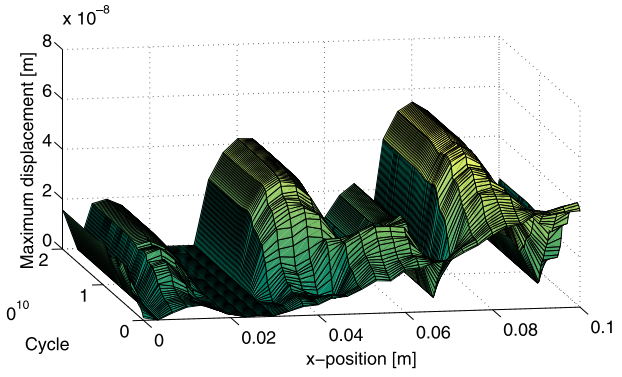

Fig. 17. Evolution of the amplitude of the horizontal displacement in the contact zone (79 kHz, $y = 0$).

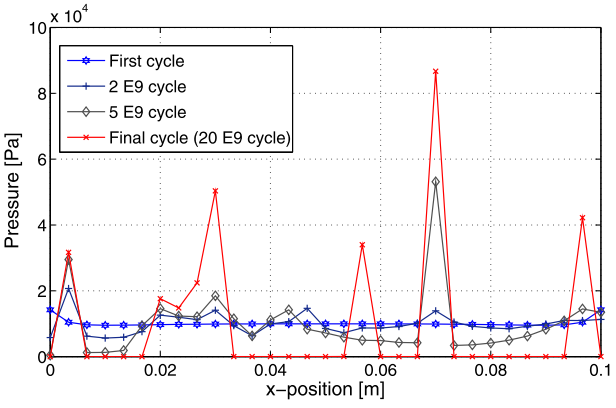

Fig. 19. Magnitude of the normal contact pressure distribution for 4 cycles (79 kHz).

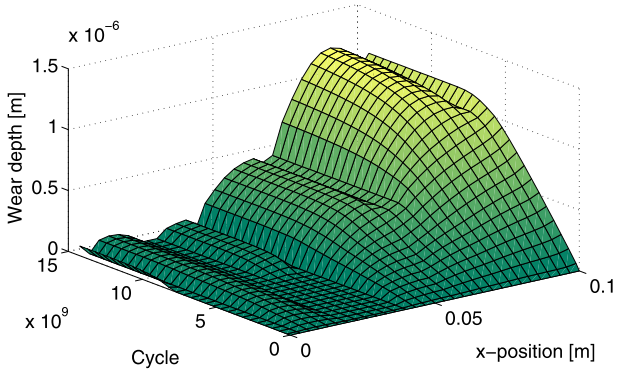

Fig. 20. Wear depth evolution (79 kHz).

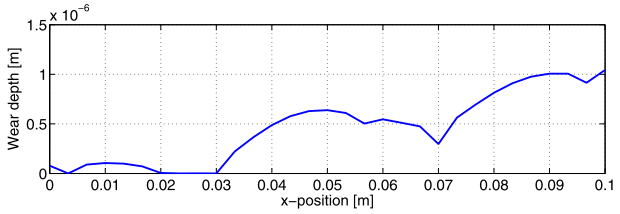

Fig. 21. Final worn profile (79 kHz).

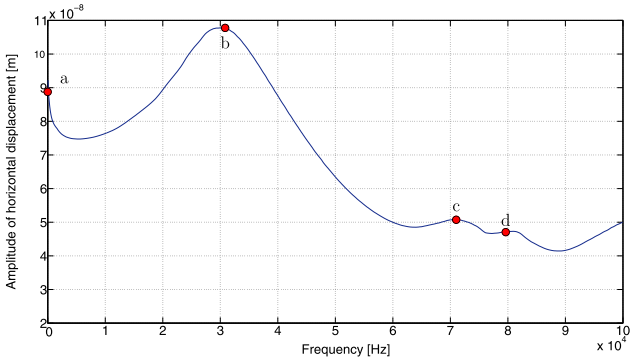

Fig. 22. Zoom on Fig. 14 for a frictional interface.

Finally, the evolution of the total worn volume appears to reveal that at 70 kHZ and 79 kHz, steady-state is reached in the dynamic case as well as for quasi-static conditions (Fig. 25). It is possible that the number of cycles tested was too low to reach such a state at 35 kHz, and that this state does not exist at this frequency. Nonetheless, it is remarkable that the evolution of the total worn volume greatly depends on frequency.

4.2.4. Comments on the numerical performance of the "DLFT with wear" method

The algorithm is implemented in a Matlab R2009 environment on a PC with a Linux OS and an Intel Core i7 920 (2.66 GHz) CPU. Statistics on the time costs of the algorithm are provided in Table 1.

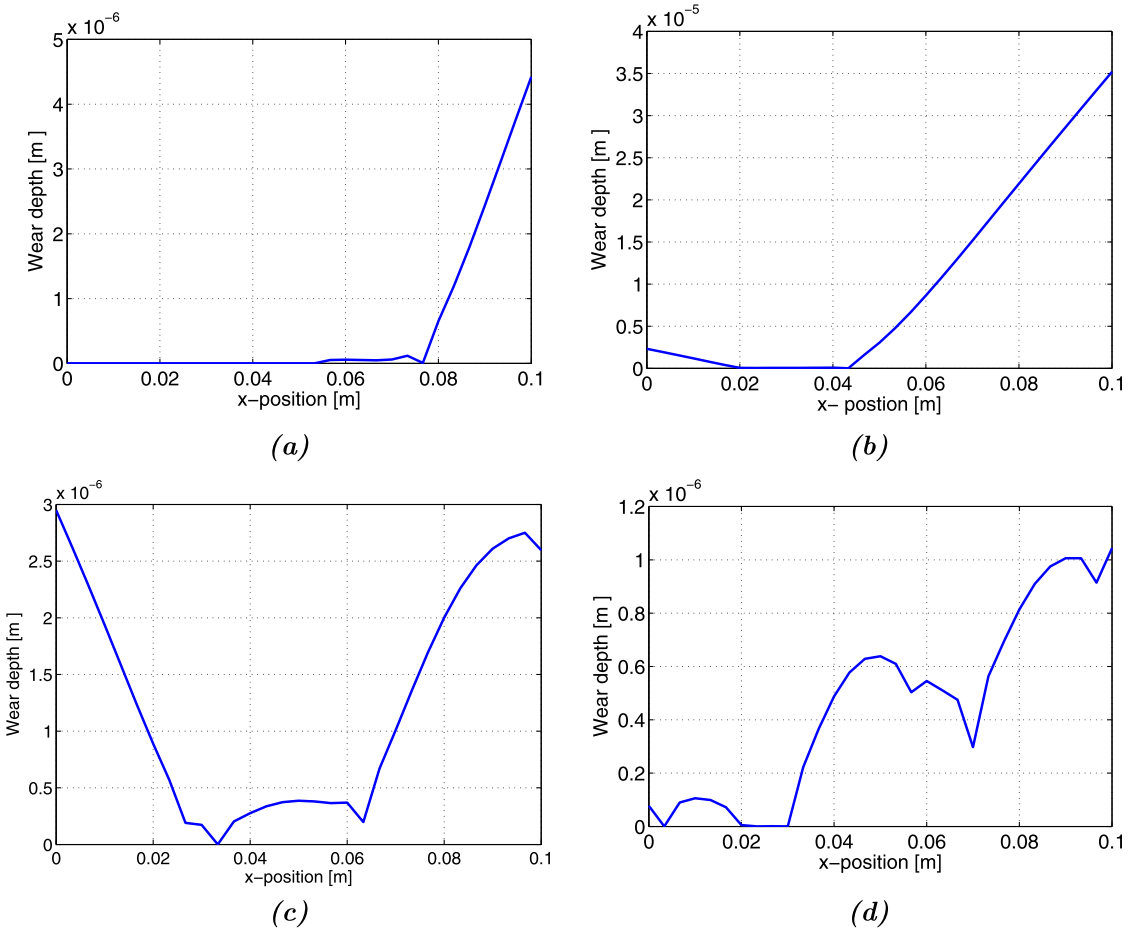

Fig. 23. Final worn profile for different frequencies: (a) quasi-static, (b) $f = 30$ kHz, (c) $f = 70$ kHz and (d) $f = 79$ kHz.

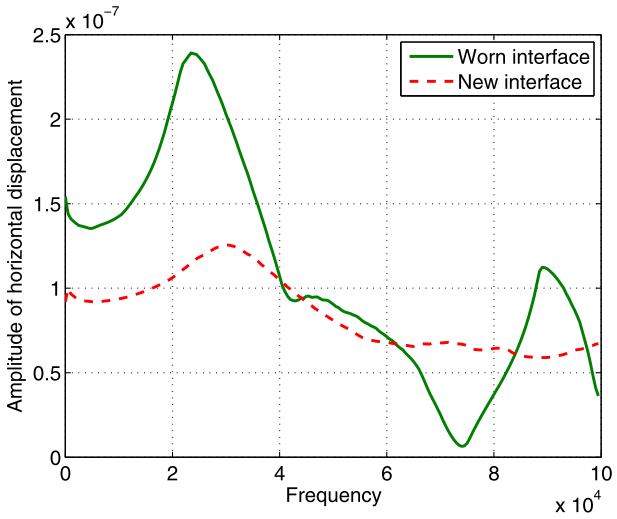

Fig. 24. Comparison of FRFs obtained with an unworn and a worn interface under frictional contact.

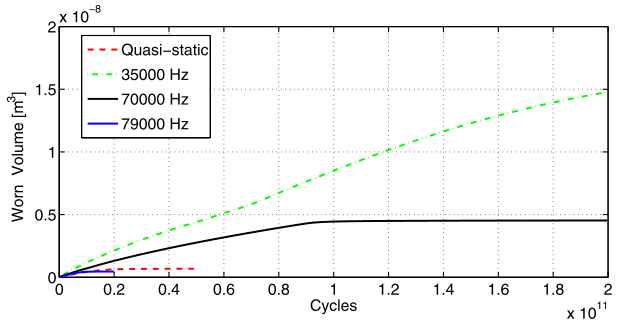

Fig. 25. Evolution of total worn volume for different frequencies.

Here, it is important to note that many wear cycles are skipped, since the evolution of the worn profile during a single cycle is very limited. Therefore, by using an explicit Euler scheme, the wear integration procedure on the slow time scale is based on increments whose maximum value is set at 1*E*8 cycles for the quasi-static case and at 1*E*7 cycles for the 79 kHz case (to ensure convergence). The total number of cycles actually dealt with in the non-linear algorithm is therefore smaller than the total number of cycles physically addressed. The cycles mentioned in the table are only those actually computed in the non-linear procedure.

The second column gives the average number of iterations required by the Newton solver in the "DLFT with wear" algorithm for the whole range of cycles covered by the calculations. A low number of iterations is generally enough but a maximum of 15 iterations has been observed. The third column shows that, on average, more CPU time is required to reach convergence for dynamic behavior than for quasi-static behavior. The other columns confirm this tendency. The evaluation of fretting-wear under vibration conditions is therefore a more time consuming procedure.

Table 1
Statistics on the performance of the "DLFT with wear" method.

Example	New. it./ cycle	CPU time/ cycle (s)	Total New. it.	Total cycle nb	Total CPU time (s)
Quasi-static	2.96	0.57	4474	1510	861
79 kHz	2.32	1.02	13977	6007	6127

5. Conclusions and prospects

In this paper, a method was proposed for simultaneously calculating the wear and vibrations of structures in fretting-wear situations. It is based on the assumption that dynamic and tribological phenomena can be separated into two time scales. The vibrations are analyzed in the frequency domain by using harmonic balance and AFT procedures. The evolution of wear is integrated on a slow time scale through an explicit scheme coupled with an approach in which cycles are skipped.

The tests performed on a two dimensional case show good agreement between the "DLFT with wear" method and a method from the literature in the quasi-static case. Nevertheless, the comparison of the quasi-static forced response with its dynamic counterparts, including inertia at different frequencies, reveals the importance of coupling between dynamics and wear and the complexity of wear kinetics. Indeed, although wear depths are very small (a few microns), they greatly modify the vibratory behavior of structures. This is why it is strongly recommended that designers take this parameter into account when designing structures subject to fretting-wear and vibratory loads. They can use the method presented here, but calibration tests must obviously be performed to guarantee that the life expectancy calculations are faithful to reality.

To conclude, a steady state with null wear rate was highlighted in the example for several loading conditions. In the future, this topic may give rise to another method, potentially based on an optimization process intended to rapidly detect asymptotic worn geometry, if it exists.

Acknowledgments

The authors thank Snecma for its technical and financial support. This work was conducted in the framework of the MAIA mechanical research and technology program sponsored by CNRS, ONERA and the SAFRAN Group.

References

Archard, J.F., 1953. Contact and rubbing of flat surfaces. Journal of Applied Physics 24 (8), 981–988.
Berthier, Y., Colombie, C., Vincent, L., Godet, M., 1988. Fretting wear mechanisms and their effects on fatigue. Journal of Tribology 110, 517–524.
Cameron, T.M., Griffin, J.H., 1989. An alternating frequency/time domain method for calculating the steady-state response of nonlinear dynamic systems. ASME, Transactions, Journal of Applied Mechanics 56, 149–154.
Charleux, D., Gibert, C., Thouverez, F., Dupeux, J., 2006. Numerical and experimental study of friction damping in blade attachments of rotating bladed disks. International Journal of Rotating Machinery 2006, 1–13.
Ciğeroğlu, E., Özgüven, H.N., 2006. Nonlinear vibration analysis of bladed disks with dry friction dampers. Journal of Sound and Vibration 295, 1028–1043.
Csaba, G., 1998. Forced response analysis in time and frequency domains of a tuned bladed disk with friction dampers. Journal of Sound and Vibration 214 (3), 395–412.
Cusumano, J.P., Chatterjee, A., 2000. Steps towards a qualitative dynamics of damage evolution. International Journal of Solids and Structures 37 (44), 6397–6417.
Demiray, H., Brommundt, E., 1997. A simple mechanism for the polygonalization of railway wheels by wear. Mechanics Research Communications 24 (4), 435–442.
Fouvry, S., Liskiewicz, T., Kapsa, P., Hannel, S., Sauger, E., 2003. An energy description of wear mechanisms and its applications to oscillating sliding contacts. Wear 255 (1–6), 287–298.
Gallego, L., Nélias, D., Jacq, C., 2006. A comprehensive method to predict wear and to define the optimum geometry of fretting surfaces. Journal of Tribology 128, 476–485.
Guillen, J., Pierre, C., 1999. An efficient, hybrid, frequency–time domain method for the dynamics of large-scale dry friction damped structural systems. In: IUTAM Symposium on Unilateral Multibody Contacts. Kluwer Academic Pub.
Hong, H.K., Liu, C.S., 2000. Coulomb friction oscillator: Modelling and responses to harmonic loads and base excitations. Journal of Sound and Vibration 229 (5), 1171–1192.
Laxalde, D., Thouverez, F., Sinou, J.J., Lombard, J.P., 2007. Qualitative analysis of forced response of blisks with friction ring dampers. European Journal of Mechanics/A Solids 26 (4), 676–687.

Laxalde, D., Salles, L., Blanc, L., Thouverez, F., 2008. Non-linear modal analysis for bladed disks with friction contact interfaces. In: Proceedings of ASME Turbo Expo.
Leonard, B.D., Sadeghi, F., Evans, R.D., Doll, G.L., Shiller, P.J., 2009. Fretting of WC/a-C:H and Cr2N coatings under grease-lubricated and unlubricated conditions. Tribology Transactions 53, 145–153.
Levy, G., 1980. Modeling of coulomb damping and wear of vibrating systems. Wear 64 (1), 57–82.
Mary, C., Fouvry, S., 2007. Numerical prediction of fretting contact durability using energy wear approach: Optimisation of finite-element model. Wear 263, 444–450.
McColl, I.R., Ding, J., Leen, S.B., 2004. Finite element simulation and experimental validation of fretting wear. Wear 256 (11), 1114–1127.
Meirovitch, L., 2004. Methods of Analytical Dynamics. Dover Publications.
Meng, H.C., Ludema, K.C., 1995. Wear models and predictive equations: Their form and content. Wear 181 (2), 443–457.
Nacivet, S., Pierre, C., Thouverez, F., Jézéquel, L., 2003. A dynamic Lagrangian frequency–time method for the vibration of dry-friction-damped systems. Journal of Sound and Vibration 265 (1), 201–219.
Nayfeh, A.H., Mook, D.T., 1979. Nonlinear Oscillations. Wiley.
Petrov, E.P., Ewins, D.J., 2002. Models of friction damping with variable normal load for time-domain analysis of vibrations. In: Proceedings of the International Conference on Noise and Vibration Engineering (ISMA), Leuven.
Petrov, E.P., Ewins, D.J., 2003. Analytical formulation of friction interface elements for analysis of nonlinear multi-harmonic vibrations of bladed disks. Journal of Turbomachinery 125, 364–371.
Põdra, P., Andersson, S., 1997. Wear simulation with the Winkler surface model. Wear 207, 79–85.
Poudou, O., Pierre, C., 2003. Hybrid frequency–time domain methods for the analysis of complex structural systems with dry friction damping. In: Collection of Technical Papers – AIAA/ASME/ASCE/AHS/ASC Structures, Structural Dynamics and Materials Conference, pp. 111–124.
Salles, L., Blanc, L., Thouverez, F., Gouskov, A.M., 2008. Dynamic analysis of fretting-wear in friction contact interfaces. In: Proceedings of ASME Turbo Expo.
Salles, L., Blanc, L., Thouverez, F., Gouskov, A.M., Jean, P., 2009. Dynamic analysis of a bladed disk with friction and fretting-wear in blade attachments. In: Proceedings of ASME Turbo Expo.
Sextro, W., 2002. Dynamical Contact Problems With Friction: Models, Methods, Experiments, and Applications. Springer.
Sfantos, G.K., Aliabadi, M.H., 2006. Wear simulation using an incremental sliding boundary element method. Wear 260, 1119–1128.
Sfantos, G.K., Aliabadi, M.H., 2006. Application of BEM and optimization technique to wear problems. International Journal of Solids and Structures 43, 3626–3642.
Soderberg, S., Bryggman, U., McCullough, T., 1986. Frequency effects in fretting wear. Wear 110, 19–34.
Stromberg, N., 1997. An augmented Lagrangian method for fretting problems. European Journal of Mechanics. A. Solids 16 (4), 573–593.